



Investigation of the effect of magnesium and activated carbon on the photocatalytic degradation reaction of ZnO photocatalyst

M. Sait Çevik^a, Ömer Şahin^b, Orhan Baytar^b, Sabit Horoz^{c,*}, Arzu Ekinci^d

^aInstitute of Science and Technology, Siirt University, Siirt 56100, Turkey

^bDepartment of Chemical Engineering, Faculty of Engineering, Siirt University, Siirt 56100, Turkey

^cDepartment of Electrical and Electronics Engineering, Faculty of Engineering, Siirt University, Siirt 56100, Turkey, email: sabithoroz@siirt.edu.tr (S. Horoz)

^dDepartment of Occupational Health and Safety, Siirt School of Health, Siirt University, Siirt 56100, Turkey

Received 16 March 2020; Accepted 17 August 2020

ABSTRACT

To improve the photodegradation of methyl blue (MB) by ZnO under visible light irradiation, the sol-gel method was used to synthesize ZnO photocatalysts co-doped with Mg and supported on activated carbon (AC) with various properties. The photocatalysts synthesized were characterized in terms of their structure and optical properties. X-ray diffraction and UV-vis absorption spectra measurements were carried out to examine the structural and optical properties of photocatalysts. Such photocatalytic behaviors of photocatalysts preceded the order: Mg:ZnO/AC > ZnO/AC > ZnO. This consequence was ascribed to the small crystallite size, large surface area, the narrow bandgap of Mg:ZnO/AC photocatalyst. Besides, first-order kinetics accompanied the degradation of MB on photocatalysis. The active species $\cdot\text{OH}$ and $\cdot\text{O}_2^-$ performed more key roles in composite photocatalytic degradation of MB.

Keywords: Activated carbon; Characterization; Doping; Photocatalytic; Synthesis

1. Introduction

Wastewaters that include reactive dyes emitted from different industries also create many environmental issues [1]. Such wastewaters enable the receiving surface water bodies to experience any damage to the ecological system [2,3]. Several studies have made considerable efforts to reach effective treatment approaches to extract toxins and contaminants from wastewater originating from various industries [4–7]. Several chemical and physical dye removal approaches have been used from the past to the present, involving membranes, adsorption strategies, and photocatalytic degradation [8–10]. Lately, photocatalytic degradation has been used by many scientists as one of the specialized oxidation processes (AOPs) to eliminate dyes

from wastewaters [11]. The photocatalytic reaction happens by illumination and catalysis with no alteration in the catalysis which may raise the reaction rates within this circumstance [12]. Semiconductors perform a catalytic task in inappropriate situations due to the low fraction energy through power and conduction bands [13]. In the photocatalytic step, the energy of two levels equally different is required adsorption of this energy that allows electrons to travel leading to hole and electron pair formation. Electrons may engage in reducing the population of electron acceptors and in the oxidation of populations of electron donors [14].

Several of the components used as photocatalysis such as TiO_2 [15], ZnO [16], ZrO_2 [17], CdS [18], MoS_2 [19], and WO_3 [20] have been used to remove the contaminants. TiO_2

* Corresponding author.

is a typical photocatalysis within these substances and has had a maximum application so far. TiO_2 has benefits, including environmental protection and non-toxicity, chemical durability, and recovery and reuse capability. Nevertheless, in the ultraviolet area, TiO_2 has complications such as high price and adsorption band. ZnO is, therefore, a good replacement for TiO_2 in the photocatalytic system [21].

Zinc oxide is one of the richest structures with a great many advantages. Thus, ZnO has many uses for various research studies [22]. Multiple technologies such as soft chemical method, sol-gel process, vapor phase production, vapor-liquid-solid mechanism, electrophoretic precipitation, thermal evaporation, homogeneous precipitation, and chemical vapor deposition were used to produce the ZnO [23–30].

For the first time in this study, therefore, the Mg-doped ZnO has been produced with modified activated carbon, and photocatalytic behavior of obtained Mg-doped ZnO has also been used to degrade methyl blue (MB) azo dye.

2. Experimental part

In a traditional synthesis, $\text{Zn}(\text{CH}_3\text{COO})_2 \cdot 2\text{H}_2\text{O}$ (0.01 mol) was dissolved for 30 min in 60 mL of $\text{C}_2\text{H}_6\text{O}$ under stirring in a water bath (60°C), and then the mixture was called solution 1. Solution 2 was formed by combining 5.040 g of $(\text{COOH})_2 \cdot 2\text{H}_2\text{O}$ in 80 mL of $\text{C}_2\text{H}_6\text{O}$ in water bath stirring for 30 min at 50°C. Solution 2 was included dropwise to the warm solution 1. The sample was dried in a vacuum stove at 80°C for 24 h. Eventually, for 2 h, ZnO was produced via thermal processing at 400°C.

For the preparation of Mg:ZnO/AC, 0.034 g of $\text{MgCl}_2 \cdot 6\text{H}_2\text{O}$, and 0.9 g of $\text{CH}_4\text{N}_2\text{O}$ was dissolved in solution 1. Then, 2.0 g AC was dispersed in 200 mL $\text{C}_2\text{H}_6\text{O}$ for 1 h under sonication and 0.2 g ZnO was dispersed in 50 mL $\text{C}_2\text{H}_6\text{O}$ for 20 min. Both solutions were intermixed and the mixture was subsequently sonicated for 1 h and then stirred for 15 h. The resulting samples were centrifuged and dried at 80°C.

The analysis of adsorption of MB on photocatalyst was conducted to evaluate the adsorption efficiency of the synthesized photocatalyst. The photocatalyst was applied to 30 mL of MB solution, then stirred the solution into the dark at for 1 h. The collected sample was filtered, and MB concentrations were calculated at 465 nm using a spectrophotometer UV5100.

In order to study the degradation of MB solution in the presence of photocatalyst, photocatalytic measurements were carried out using a 500 W Xe lamp as the visible light source. Xe lamp power was kept at 500 W and preserved an overall irradiation strength of 350 W/m^2 across the tests. The photocatalyst was transferred to the solution of MB. The solution was consistently stirred and held for 1 h in the dark to permit an adsorption-desorption balance between MB and the photocatalyst. The suspension was subsequently displayed under visible light to eliminate MB. Each sample was subsequently extracted after degradation test to avoid photocatalyst for examination.

X-ray diffractometer (Rigaku XRD), energy dispersive X-ray (EDX; JEOL JSM 5800), and UV-vis absorption spectra (Perkin Elmer Lambda 2 spectrometer, Waltham, Massachusetts, US)

measurements were carried out to examine the structural, elemental, and optical properties of photocatalysts.

3. Results and discussion

Fig. 1 indicates the photocatalytic degradation of MB in the presence of AC-supported ZnO photocatalysts with different AC concentrations (5%, 10%, and 20%). *Experiment conditions:* the MB solution volume is 30 mL, the MB concentration is 10 ppm, the pH of the system is 6, and the amount of photocatalyst is 10 mg.

As seen in Fig. 1, photocatalytic degradation of MB is completed within 98 min in the presence of pure ZnO photocatalyst, whereas in the presence of AC-supported ZnO photocatalyst, the same reaction was observed to end within 50 min. The probable reason for this is that ZnO is attached to a support material with a large surface area, such as AC, to increase its active surface area. Another reason is thought to be accelerating the electron circulation in the environment due to the conductivity structure of AC. Moreover, as clearly seen in Fig. 1, when the AC ratio was increased from 5% to 10%, it was observed that the degradation experiment was completed sooner. However, it was observed that the reaction completion time increases when the AC ratio is increased by up to 20%. The reason for the longer reaction time when the AC ratio is 20% can be considered as the saturation of the active surface area. Thus, in the light of the results shown in Fig. 1, in the presence of AC-supported ZnO photocatalyst with different AC concentrations, the optimum AC ratio was determined as 10% in this study, and the synthesized sample was named as ZnO/AC.

After determining the optimum AC ratio, the ZnO/AC photocatalyst was doped with different Mg concentrations (0%, 0.4%, 0.8%, 1.2%, 1.6%, and 2%) to enhance its photocatalytic activity. Fig. 2 points out the photocatalytic degradation of MB in the presence of ZnO/AC photocatalyst doped

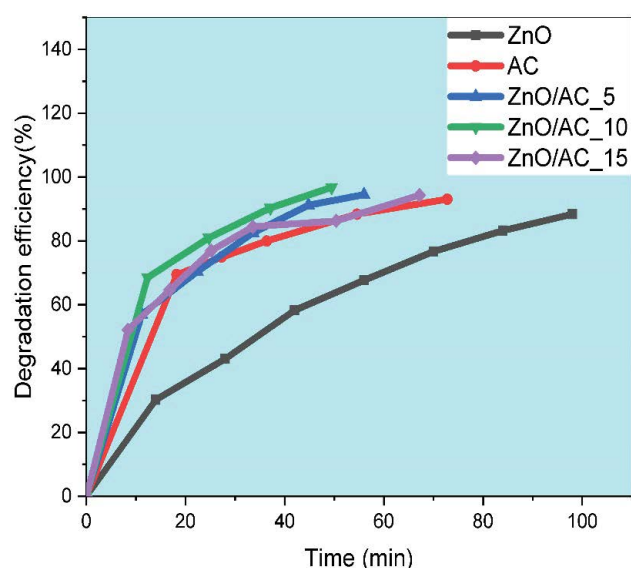


Fig. 1. Photocatalytic degradation of MB in the presence of AC-supported ZnO photocatalysts with different AC concentrations (5%, 10%, and 20%).

with different Mg concentrations. *Experiment conditions:* the MB solution volume is 30 mL, the MB concentration is 10 ppm, the pH of the system is 6, and the amount of photocatalysts is 10 mg.

In Fig. 2, it is seen that photocatalytic activities of Mg-doped ZnO/AC photocatalysts are better than ZnO/AC photocatalysts. The activity of these photocatalysts is considered to be high since the Mg-doped metal increases the number of active sites on the surface of the ZnO/AC photocatalyst. It was found that when the metal concentration was increased from 0.4% to 1.6%, the reaction of Mg-doped ZnO/AC photocatalyst was completed in a shorter time, but the reaction time was longer when the metal ratio was increased up to 2%. The probable reason for this is that the high Mg concentration decreases the number of active regions of the photocatalyst. Thus, in the light of the results shown in Fig. 2, in the presence of ZnO/AC photocatalyst doped with different Mg concentrations, the optimum metal ratio was determined as 1.6% in this current study and the synthesized sample was named as Mg:ZnO/AC.

In the presence of Mg:ZnO/AC photocatalyst, using different MB concentrations, photocatalytic degradation experiments of MB were carried out and the effect of MB concentration was investigated. *Experiment conditions:* the MB solution volume is 30 mL, the MB concentration is 10, 20, 50, and 100 ppm, the pH of the system is 6, and the amount of photocatalysts is 10 mg. The plot of degradation efficiency vs. time for Mg:ZnO/AC photocatalyst using the different MB concentration is revealed in Fig. 3.

The photocatalytic degradation reaction rate of MB appears to decrease with increasing concentration of MB. Increasing MB concentration rises the adsorption capacity on the Mg:ZnO/AC photocatalyst surface, which reduces the photocatalytic degradation reaction rate by preventing the OH⁻ adsorption occurring on the photocatalyst surface. As a result, the decrease in OH⁻ formation leads to a

decrease in color removal efficiency. Moreover, based on Lambert–Beer law, the increase in the initial dye concentration decreases the photon penetration into the solution and less photon adsorption occurs on the photocatalyst surface. As a result, there is a lower reaction rate.

In the presence of Mg:ZnO/AC photocatalyst, using different photocatalyst amounts, photocatalytic degradation experiments of MB were carried out and the effect of photocatalyst amount was examined. *Experiment conditions:* the MB solution volume is 30 mL, the MB concentration is 10 ppm, the pH of the system is 6, and the amount of photocatalysts is 5, 7, 10, and 15 mg. The plot of degradation efficiency vs. time for Mg:ZnO/AC photocatalyst using the different photocatalyst amounts is revealed in Fig. 4.

The fastest degradation of MB at 10 mg of photocatalyst loading in which took only 20 min to complete the reaction. On the other hand, the other catalyst loading was able to degrade within the longer irradiation time. According to Fig. 4, 10 mg of photocatalyst loading shown the highest photodegradation performance which is 98.81% while 5, 7, and 15 mg of photocatalyst loading resulting in 92.44%, 94.90%, and 95.88% degradation of MB, respectively. The results suggest that the degradation performance increases proportionally with the catalyst loading. The best catalyst loading for the photocatalytic degradation of MB in the presence of Mg:ZnO/AC photocatalyst is 10 mg. However, at higher catalyst loading (15 mg), it was observed that the degradation efficiency decreased because of agglomeration and thus lower the photocatalytic activity.

In the presence of Mg:ZnO/AC photocatalyst, using different pH values, photocatalytic degradation experiments of MB were carried out and the effect of pH of the system was examined. *Experiment conditions;* the MB solution volume is 30 mL, the MB concentration is 10 ppm, the pH of the system is 2, 4, 6, 8, and 10, and the amount of photocatalysts is 10 mg. The plot of degradation efficiency

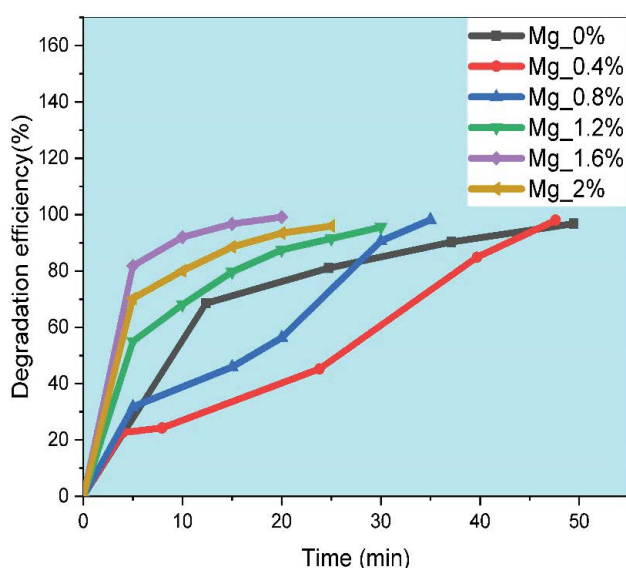


Fig. 2. Photocatalytic degradation of MB in the presence of ZnO/AC photocatalyst doped with different Mg concentrations (0%, 0.4%, 0.8%, 1.2%, 1.6%, and 2%).

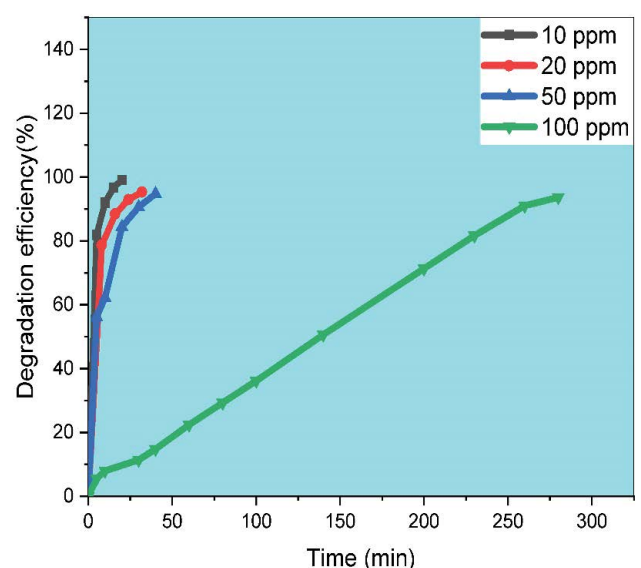


Fig. 3. Photocatalytic degradation of MB in the presence of Mg:ZnO/AC photocatalyst using different MB concentrations (10, 20, 50, and 100 ppm).

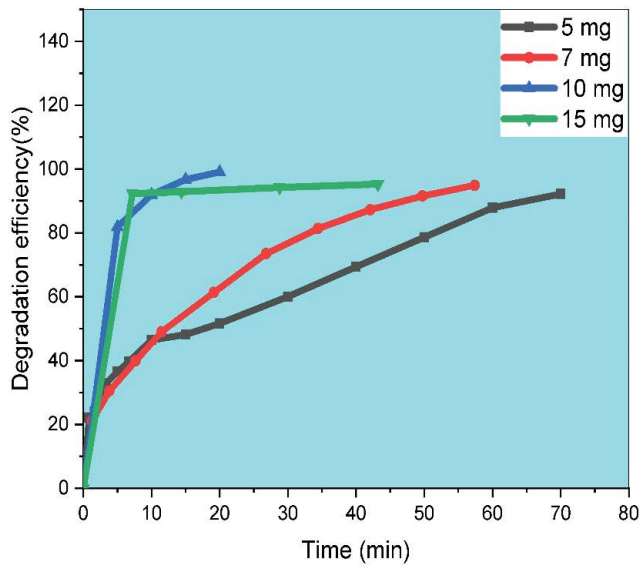


Fig. 4. Photocatalytic degradation of MB in the presence of Mg:ZnO/AC photocatalyst using different photocatalyst amounts (5, 7, 10, and 15 mg).

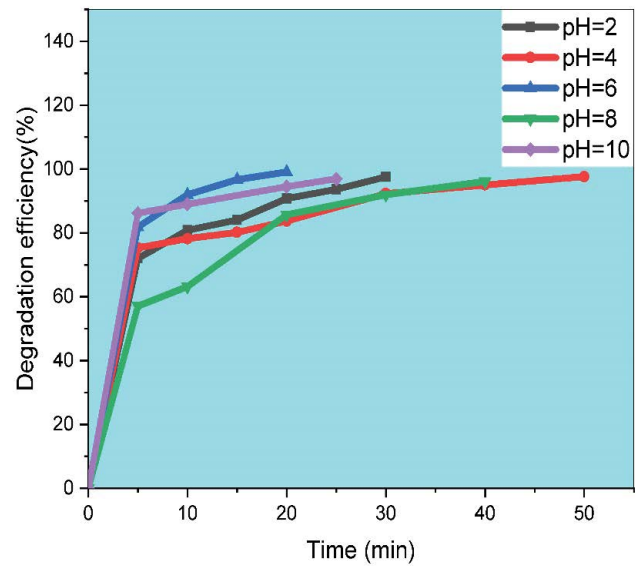


Fig. 5. Photocatalytic degradation of MB in the presence of Mg:ZnO/AC photocatalyst using different pH values (2, 4, 6, 8, 10).

vs. time for Mg:ZnO/AC photocatalyst using the different pH values is indicated in Fig. 5.

The pH value of the system is one of the main reasons affecting the photocatalytic degradation reaction. As seen in Fig. 5, the photocatalytic degradation efficiency of MB enhances with increasing pH value. The probable reason for this is the improvement in photocatalytic degradation efficiency due to the rise in the number of OH⁻ ions in the environment with increasing pH value.

In the presence of Mg:ZnO/AC photocatalyst, the photocatalytic degradation kinetics of MB was examined with the first and second-order-kinetic model. First and second-order-kinetic model equations are given below:

$$-\ln\left(\frac{C_t}{C_0}\right) = k_1 \cdot t \quad (1)$$

$$\frac{1}{C_t} - \frac{1}{C_0} = k_2 \cdot t \quad (2)$$

where C_t is the solution concentration at the time t (mg/L), C_0 is the initial solution concentration (mg/L), k_1 is the first-order adsorption rate constant (1/min), k_2 is the second-order adsorption rate constant (1/min), t is the adsorption time (min.)

The plots obtained from the above equations for the first and second-order-kinetic model are given in Figs. 6a and b, respectively.

The k_1 /regression and k_2 /regression coefficients of Mg:ZnO/AC photocatalyst were determined as 0.159 (1/min)/0.948 and 0.067 (1/min)/0.934, respectively. According to the regression coefficient, it was observed that the photocatalytic degradation kinetics of MB fits the first-order-kinetic model better.

The XRD peaks of all designed photocatalyst are presented in Fig. 7.

The patterns obtained correspond to the planes (100), (002), (101), (102), (110), and (103) of the ZnO hexagonal structure. All applicable diffraction data for ZnO corresponded well to the data provided (JCPDS 36-1451). All photocatalysts have identical XRD patterns, which meant that the addition of Mg and AC does not affect ZnO's phase structure. Nevertheless, the XRD patterns of Mg:ZnO/AC photocatalyst did not show any apparent characteristic diffraction peaks of Mg, which could be due to the low doping level. Additionally, in their reports, Bhirud et al. [31] documented the phenomenon. Furthermore, the characteristic diffraction peak of AC was not observed in Mg:ZnO/AC photocatalyst because of the comparatively low diffraction strength of AC. Compared with ZnO, the pattern intensity of Mg:ZnO/AC photocatalyst decreased, which was relative to the lower concentration of crystalline material (ZnO) in a matrix of amorphous matter (AC).

The average crystallite sizes of the ZnO, ZnO/AC, and Mg:ZnO/AC photocatalysts were calculated as 16.8, 14.3, and 11.6 nm, respectively, using the Debye-Scherrer formula from hexagonal wurtzite (101) peaks. ZnO/AC and Mg:ZnO/AC photocatalysts had smaller crystallite sizes than ZnO since AC behaves as a gap to crystal growth's limiter action. Mg:ZnO/AC's crystallite size was 11.6 nm, the smallest of all photocatalysts. Smaller particle size may be beneficial to improve the photocatalytic behavior of photocatalyst.

Using UV vis diffuse absorption spectra, the photoabsorption activity of the synthesized ZnO, ZnO/AC, and Mg:ZnO/AC photocatalysts were studied. The wavelength (nm) vs. intensity (a.u.) plots for photocatalysts are shown in Fig. 8a. The graph of $(\alpha h\nu)^{1/2}$ vs. the energy of light (hν), indicated in Fig. 8b, was used to determine the bandgap values of synthesized ZnO, ZnO/AC, and Mg:ZnO/AC

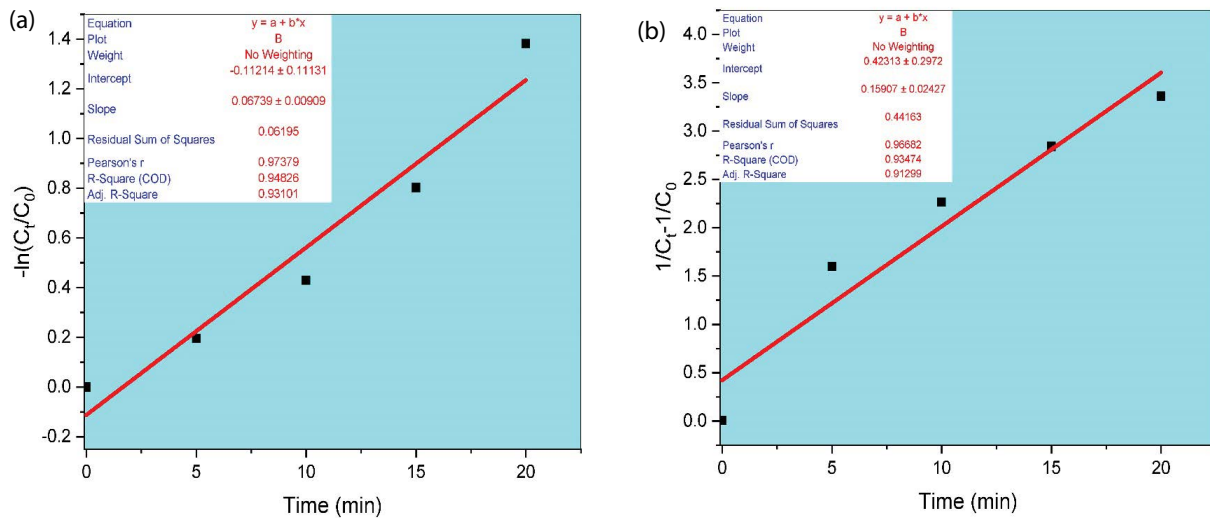


Fig. 6. (a) First-order-kinetic and (b) second-order-kinetic model for the photocatalytic degradation of MB in the presence of Mg:ZnO/AC photocatalyst.

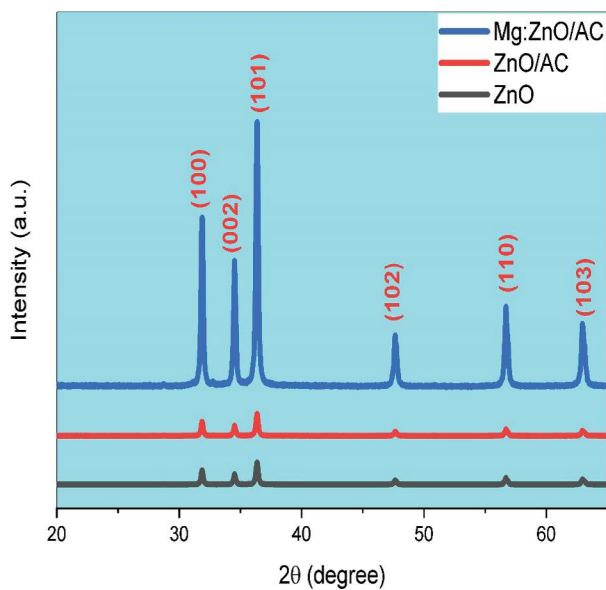


Fig. 7. XRD patterns of ZnO, ZnO/AC, and Mg:ZnO/AC photocatalysts.

photocatalysts. The determined bandgap value for ZnO, ZnO/AC, and Mg:ZnO/AC photocatalysts is 3.32, 2.92, and 2.76 eV, respectively.

This observation might be explained by the fact that Mg:ZnO/AC has an extensive pore configuration which induces light to scatter inside and AC to absorb at wavelengths slightly higher than pure ZnO. In comparison to the pure ZnO, the Mg:ZnO/AC photocatalyst's band edge absorption was red-shifted and demonstrated broad absorption in the visible-light area, which can be related to the movement of load between the Mg 3d state along with to the ZnO conduction or valance bands. Thus the absorption edge is expanded to visible light, resulting in the production of electron-hole couples, which improves the photocatalytic

capabilities of the Mg:ZnO/AC photocatalyst. The charging of the Mg:ZnO on AC gives rise to a narrowing of the band-gap and an increase in absorbance in the visible zone, which is probably as a result of the formation of Zn–O–C as well as carbon doping ZnO [32].

EDX spectra of ZnO/AC and Mg:ZnO/AC photocatalysts are demonstrated in Figs. 9a and b, respectively. Fig. 8b obviously indicates the presence of C, Zn, Mg, and O ions in Mg:ZnO/AC photocatalyst. This confirms the successful doping process.

4. Conclusions

In the first stage of the present study, photocatalytic degradation experiments of MB were carried out in the presence of AC-supported ZnO photocatalysts with different AC concentrations synthesized using sol-gel technique. The photocatalytic degradation rate of 5% AC-supported ZnO (ZnO/AC) photocatalyst was found to be higher compared to other concentrations.

In the second stage of the study, ZnO/AC photocatalyst was doped with different concentrations of Mg metal. As a result of photocatalytic degradation experiments of MB, it was observed that the degradation reaction was completed in a shorter time in the presence of 1.6% Mg-doped ZnO/AC (Mg:ZnO/AC) photocatalyst compared to other concentrations.

In the third stage of the study, it was investigated how some parameters (MB concentration, photocatalyst amount, and pH of the system) affect the photocatalytic degradation reaction of methylene blue in the presence of Mg:ZnO/AC photocatalyst. The graphics obtained were interpreted.

In the last stage of the study, the structural and optical properties of Mg:ZnO/AC photocatalyst were examined. It was observed that Mg (1.6%) and AC (5%) did not change the structure of ZnO, which has a hexagonal structure, but the crystalline size of ZnO decreased due to AC (5%) and Mg (1.6%). Besides, the Mg:ZnO/AC (2.76 eV) photocatalyst was found to have a narrower energy band gap than ZnO (3.32 eV) and ZnO/AC (2.92 eV) photocatalysts.

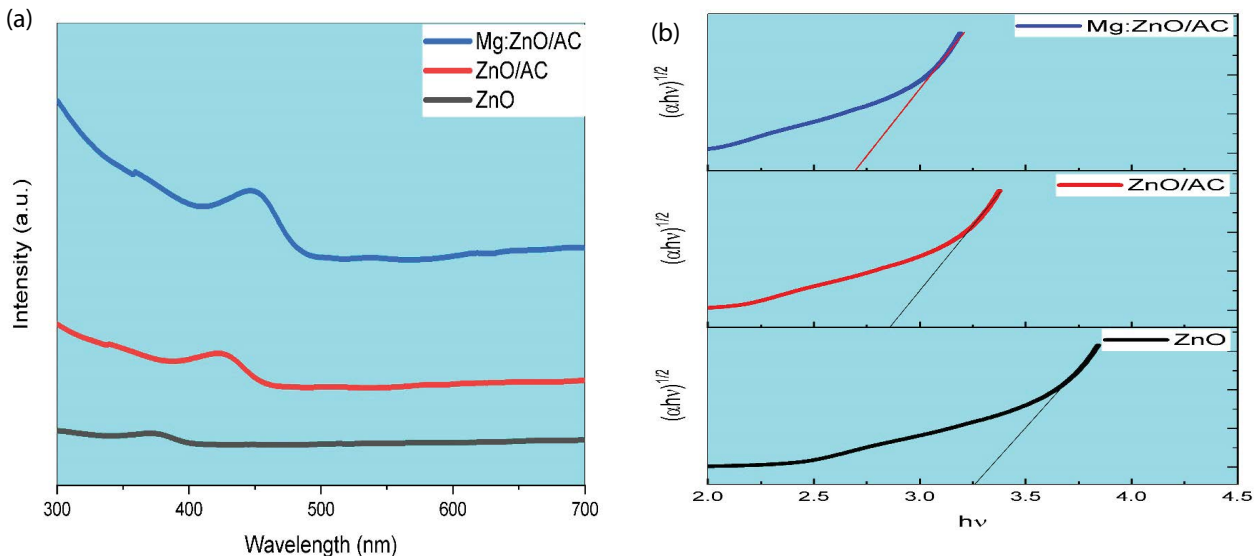


Fig. 8. (a) Plot of absorbance intensity vs. wavelength and (b) plot of $(\alpha h\nu)^{1/2}$ vs. $h\nu$ for ZnO, ZnO/AC, and Mg:ZnO/AC photocatalysts.

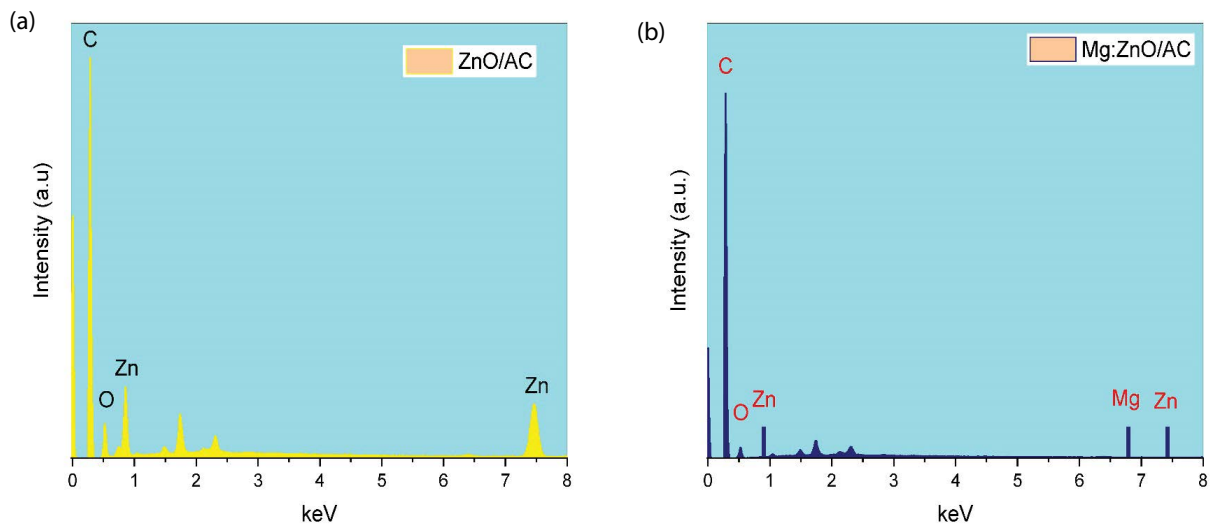


Fig. 9. EDX spectra of (a) ZnO/AC and (b) Mg:ZnO/AC photocatalyst.

As a result, such photocatalytic behaviors of photocatalysts preceded the order: Mg:ZnO/AC > ZnO/AC > ZnO. This consequence was ascribed to the small crystallite size, large surface area, the narrow bandgap of Mg:ZnO/AC photocatalyst.

Acknowledgments

The authors are grateful to the Research Foundation of Siirt University for financial support under project 2019-SİÜFEB-019.

References

- [1] S. Horoz, O. Baytar, O. Sahin, H. Kilicvuran, Photocatalytic degradation of methylene blue with Co alloyed CdZnS nanoparticles, *J. Mater. Sci. Mater.*, 29 (2018) 1004–1010.
- [2] O. Baytar, O. Sahin, H. Kilicvuran, S. Horoz, Synthesis, structural, optical and photocatalytic properties of Fe-alloyed CdZnS nanoparticles, *J. Mater. Sci. Mater.*, 29 (2018) 4564–4568.
- [3] M.-h. Wu, J. Li, G. Xu, L.-d. Ma, J.-j. Li, J.-s. Li, L. Tang, Pollution patterns and underlying relationships of benzophenone-type UV-filters in wastewater treatment plants and their receiving surface water, *Ecotoxicol. Environ. Saf.*, 152 (2018) 98–103.
- [4] A. Ahmad, S.H. Mohd-Setapar, C.S. Chuong, A. Khatoun, W.A. Wani, R. Kumar, M. Rafatullah, Recent advances in new generation dye removal technologies: novel search for approaches to reprocess wastewater, *RSC Adv.*, 5 (2015) 30801–30818.
- [5] Z. Al-Qodah, M. Al-Shannag, Heavy metal ions removal from wastewater using electrocoagulation processes: a comprehensive review, *Sep. Sci. Technol.*, 52 (2017) 2649–2676.
- [6] G. Crini, E. Lichtfouse, Advantages and disadvantages of techniques used for wastewater treatment, *Environ. Chem. Lett.*, 17 (2019) 145–155.
- [7] D.T. Moussa, M.H. El-Naas, M. Nasser, M.J. Al-Marri, A comprehensive review of electrocoagulation for water

- treatment: potentials and challenges, *J. Environ. Manage.*, 186 (2017) 24–41.
- [8] W.S. Koe, J.W. Lee, W.C. Chong, Y.L. Pang, L.C. Sim, An overview of photocatalytic degradation: photocatalysts, mechanisms, and development of photocatalytic membrane, *Environ. Sci. Pollut.*, 27 (2020) 2522–2565.
- [9] A. Mudhoo, A. Bhatnagar, M. Rantalankila, V. Srivastava, M. Sillanpää, Endosulfan removal through bioremediation, photocatalytic degradation, adsorption and membrane separation processes: a review, *Chem. Eng. J.*, 360 (2019) 912–928.
- [10] K. Singh, S. Arora, Removal of synthetic textile dyes from wastewaters: a critical review on present treatment technologies, *Crit. Rev. Environ. Sci. Technol.*, 41 (2011) 807–878.
- [11] Y. Deng, R. Zhao, Advanced oxidation processes (AOPs) in wastewater treatment, *Curr. Pollut. Rep.*, 1 (2015) 167–176.
- [12] T. Yao, X. An, H. Han, J.Q. Chen, C. Li, Photoelectrocatalytic materials for solar water splitting, *Adv. Energy Mater.*, 8 (2018) 1–36, doi: 10.1002/aenm.201800210.
- [13] K. Parida, S. Dash, D. Das, Physico-chemical characterization and photocatalytic activity of zinc oxide prepared by various methods, *J. Colloid Interface Sci.*, 298 (2006) 787–93.
- [14] M. Nasrollahzadeh, M. Hadavifar, S. Ghasemi, M. Chamjangali, Synthesis of ZnO nanostructure using activated carbon for photocatalytic degradation of methyl orange from aqueous solutions, *Appl. Water Sci.*, 8 (2018) 1–12, doi: 10.1007/s13201-018-0750-6.
- [15] V. Etacheri, C. Di Valentin, J. Schneider, D. Bahnemann, S.C. Pillai, Visible-light activation of TiO₂ photocatalysts: advances in theory and experiments, *J. Photochem. Photobiol., C*, 25 (2015) 1–29.
- [16] M. Shekofteh-Gohari, A. Habibi-Yangjeh, M. Abitorabi, A. Rouhi, Magnetically separable nanocomposites based on ZnO and their applications in photocatalytic processes: a review, *Crit. Rev. Environ. Sci. Technol.*, 48 (2018) 806–857.
- [17] V.R. Reddy, D.W. Hwang, J.S. Lee, Photocatalytic water splitting over ZrO₂ prepared by precipitation method, *Korean J. Chem. Eng.*, 20 (2003) 1026–1029.
- [18] B. Poornaprakash, U. Chalapathi, P.T. Poojitha, S.V. Prabhakar Vattikuti, S.-H. Park, CdS:Eu quantum dots for spintronics and photocatalytic applications, *J. Mater. Sci. Mater.*, 30 (2019) 8220–8225.
- [19] Z. Li, X. Meng, Z. Zhang, Recent development on MoS₂-based photocatalysis: a review, *J. Photochem. Photobiol., C*, 35 (2018) 39–55.
- [20] C. Sotelo-Vazquez, R. Quesada-Cabrera, M. Ling, D.O. Scanlon, A. Kafizas, P.K. Thakur, T.-L. Lee, A. Taylor, G.W. Watson, R.G. Palgrave, J.R. Durrant, C.S. Blackman, I.P. Parkin, Photocatalysis: evidence and effect of photogenerated charge transfer for enhanced photocatalysis in WO₃/TiO₂ heterojunction films: a computational and experimental study, *Adv. Funct. Mater.*, 27 (2017) 1–10, doi: 10.1002/adfm.201770108.
- [21] C.B. Ong, L.Y. Ng, A.W. Mohammad, A review of ZnO nanoparticles as solar photocatalysts: synthesis, mechanisms and applications, *Renewable Sustainable Energy Rev.*, 81 (2018) 536–551.
- [22] Ü. Özgür, Y.I. Alivov, C. Liu, A. Teke, M.A. Reshchikov, S. Doğan, V. Avrutin, S.-J. Cho, H. Morkoç, A comprehensive review of ZnO materials and devices, *J. Appl. Phys.*, 98 (2005) 1–104, doi: 10.1063/1.1992666.
- [23] D. Barreca, G. Carraro, A. Gasparotto, C. Maccato, T. Altantzis, C. Sada, K. Kaunisto, T.-P. Ruoko, S. Bals, Vapor phase fabrication of nanoheterostructures based on ZnO for photoelectrochemical water splitting, *Adv. Mater. Interfaces*, 4 (2017) 1–9, doi: 10.1002/admi.201700161.
- [24] Y.-C. Chen, C.-H. Lin, T.-F. Guo, T.-C. Wen, Surfactant-enriched ZnO surface via sol-gel process for the efficient inverted polymer solar cell, *ACS Appl. Mater. Interfaces*, 10 (2018) 26805–26811.
- [25] J. Karbowiczek, L. Cordero-Arias, S. Virtanen, S.K. Misra, E. Valsami-Jones, L. Tuchscher, B. Rutkowski, K. Górecki, P. Bała, A. Czyrska-Filemonowicz, A.R. Boccaccini, Electro-phoretic deposition of organic/inorganic composite coatings containing ZnO nanoparticles exhibiting antibacterial properties, *Mater. Sci. Eng., C*, 77 (2017) 780–789.
- [26] M. Mohammadi, S. Sabbaghi, H. Sadeghi, M.M. Zerafat, R. Pooladi, Preparation and characterization of TiO₂/ZnO/CuO nanocomposite and application for phenol removal from wastewaters, *Desal. Water Treat.*, 57 (2016) 799–809.
- [27] M. Rashad, N.M. Shaalan, A.M. Abd-Elnaiem, Degradation enhancement of methylene blue on ZnO nanocombs synthesized by thermal evaporation technique, *Desal. Water Treat.*, 57 (2016) 26267–26273.
- [28] K. Saravanakumar, K. Ravichandran, Synthesis of heavily doped nanocrystalline ZnO:Al powders using a simple soft chemical method, *J. Mater. Sci. Mater.*, 23 (2012) 1462–1469.
- [29] Y.-F. Yao, K.-P. Chou, H.-H. Lin, C.-C. Chen, Y.-W. Kiang, C.C. Yang, Polarity control in growing highly Ga-doped ZnO nanowires with the vapor-liquid-solid process, *ACS Appl. Mater. Interfaces*, 10 (2018) 40764–40772.
- [30] Z. Zhan, L. Xu, J. An, H. Du, Z. Weng, W. Lu, Direct catalyst-free chemical vapor deposition of ZnO nanowire array UV photodetectors with enhanced photoresponse speed, *Adv. Eng. Mater.*, 19 (2017) 1–9, doi: 10.1002/adem.201700101.
- [31] A. Bhirud, S. Sathaye, R. Waichal, C.-J. Park, B. Kale, *In situ* preparation of N-ZnO/graphene nanocomposites: excellent candidate as a photocatalyst for enhanced solar hydrogen generation and high performance supercapacitor electrode, *J. Mater. Chem. A*, 3 (2015) 17050–17063.
- [32] X. Chen, Z. Gao, B.-C. Ye, Effect of different activated carbon as carrier on the photocatalytic activity of Ag-N-ZnO photocatalyst for methyl orange degradation under visible light irradiation, *Nanomaterials*, 7 (2017) 240–258, doi: 10.3390/nano7090258.